Protein Cell, 2025, **16**, 782–798
https://doi.org/10.1093/procel/pwaf020
Advance access publication 25 February 2025
Research Article

Protein & Cell

Research Article

Neutrophil extracellular traps license macrophage production of chemokines to facilitate CD8⁺ T cell infiltration in obstruction-induced renal fibrosis

Hongshuai Jia[1,2,‡], Guang Yue[1,2,‡], Pin Li[1,3,‡], Renjun Peng[4], Ruyue Jin[1,3], Yuhan Chen[3], Hualin Cao[5], Kangning Yang[6], Xiaowei Zhang[1], Xiaoyu Yi[1], Yangyang Wu[1,2], Xiangling Deng[1], Xiaoye Chen[5], Lifei Ma[1], Yang Zhao[1], Xiaoguang Zhou[1], Tian Tao[1], Xiaoli Shen[1], Xu Zhang[7,*], Yuandong Tao[1,3,*], Huixia Zhou[1,3,*]

[1]Department of Pediatric Urology, The Seventh Medical Center of Chinese PLA General Hospital, Beijing 100010, China
[2]Medical School of Chinese PLA, Beijing 100010, China
[3]National Engineering Laboratory for Birth Defects Prevention and Control of Key Technology, Beijing 100010, China
[4]The PLA Rocket Force Characteristic Medical Center, Beijing 100010, China
[5]Nanxishan Hospital of Guangxi Zhuang Autonomous Region, The Second People's Hospital of Guangxi Zhuang Autonomous Region, Guilin 541002, China
[6]Sichuan Mianyang 404 Hospital, Mianyang 621000, China
[7]Department of Urology, The Third Medical Center of Chinese PLA General Hospital, Beijing 100010, China

[‡]These authors contributed equally to the study.
[*]Correspondence: xzhang301@163.com (X. Zhang), tao_yuandong@163.com (Y. Tao), huixia99999@163.com (H. Zhou)

Abstract

Renal fibrosis is a common mechanism leading to kidney failure in chronic kidney diseases (CKDs), including obstructive nephropathy (ON). Dysregulated inflammation is central to the development of renal fibrosis, but how local immune cells within the tissue microenvironment integrate and coordinate to drive this condition remains largely unknown. Herein, we documented that neutrophils were abundantly recruited and expelled neutrophil extracellular traps (NETs) in human and mouse fibrotic kidneys. Importantly, circulating levels of NETs components displayed a significant correlation with worsened kidney function in ON patients. In the unilateral ureteral obstruction (UUO) mouse model, blocking NETs by protein-arginine deiminase type 4 (PAD4) deletion or DNase treatment significantly impaired NETs formation and inhibited renal fibrosis and inflammation, whereas NETs adoptive transfer exacerbated the fibrotic process. Moreover, NET-mediated renal fibrosis was associated with enhanced infiltration of cytotoxic CD8⁺ T cells, which produced granzyme B (GZMB) to drive tubular cell epithelial-mesenchymal transition (EMT) and fibroblast activation. Accordingly, pharmacological inhibition of GZMB resulted in blunted kidney inflammation and fibrosis. Furthermore, NETs profoundly potentiated the production of T-cell chemokines CXCL9/10/11 in macrophages, but not in tubular cells or fibroblasts, thus driving T-cell infiltration and fueling inflammatory cascades in the kidneys. Mechanistically, the NET-macrophage interaction was partially mediated by the TLR2/4 signaling. Thus, our work reveals a previously unexplored role of the collaboration between NETs and macrophages in supporting CD8⁺ T cell infiltration, which orchestrates kidney inflammation and fibrosis.

Keywords obstructive nephropathy, renal fibrosis, neutrophil extracellular traps, CD8⁺ T cells, granzyme B, macrophages

Received 11 December 2024; **accepted** 6 February 2025.

Introduction

Renal fibrosis is a progressive process characterized by excessive deposition of extracellular matrix (ECM) in chronic kidney diseases (CKDs), affecting more than 10% of the world's population (Kalantar-Zadeh et al., 2021; Li et al., 2022a; Wang et al., 2023). It is widely considered a common mechanism leading to end-stage renal disease, a life-threatening condition that requires kidney transplantation or hemodialysis (Ruiz-Ortega et al., 2020). Obstructive nephropathy (ON) is a major cause of CKDs and renal fibrosis, which can occur in patients with chronic urinary tract obstruction, including congenital anatomical abnormalities, renal calculi, prostatic hyperplasia, and bladder tumors (Stevens, 2018). Unfortunately, targeted therapy for renal fibrosis is limited.

Obstruction-induced kidney injury elicits inflammation as a protective response. The injured kidney tissues release damage-associated molecular patterns (DAMPs), which stimulate infiltration and activation of innate and adaptive immune cells into the kidney, including neutrophils, macrophages, and T cells (Liu, 2011). Properly regulated inflammation plays a critical role in normal tissue repair after kidney injury, but chronic and unresolved inflammation drives the development of CKDs and renal fibrosis (Lv et al., 2018). The immune cells produce a myriad of pro-inflammatory and pro-fibrotic factors to mediate tissue damage and prolonged myofibroblast activation, causing excessive ECM deposition and ultimately renal fibrosis (Lv et al., 2018). However, how these local immune cells in the fibrotic microenvironment integrate and coordinate to drive kidney inflammation and fibrosis remains largely unknown.

Neutrophil extracellular traps (NETs) are neutrophil-derived web-like structures composed mainly of double-stranded DNA (dsDNA), histones, granular proteases, and cytokines, which are always triggered by pathogens and endogenous stimuli, such as DAMPs (Papayannopoulos, 2018). The formation of NETs is regulated by protein-arginine deiminase type 4 (PAD4), which is required for chromatin decondensation, the key step of NET formation (Papayannopoulos, 2018). It has been well-described that NETs play crucial roles in infections, tumors, thrombosis, autoimmune diseases, and tissue injuries (Hidalgo et al., 2022). Notably, increasing evidence suggests that dysregulation between the production and clearance of NETs is associated with the pathophysiology of kidney diseases (Nakazawa et al., 2018; Salazar-Gonzalez et al., 2019). NETs are capable of damaging surrounding tissues and promoting inflammation in ischemia and reperfusion kidney injury (Jansen et al., 2017; Nakazawa et al., 2017), diabetic nephropathy (Wong et al., 2015; Zheng et al., 2022), and hypertensive nephropathy (Avery et al., 2023). They also serve as a source of self-antigen in autoimmune diseases, such as antineutrophil cytoplasmic autoantibody (ANCA)-associated vasculitis and lupus nephritis (Garcia-Romo et al., 2011; Hakkim et al., 2010; Tang et al., 2015). Moreover, recent research has revealed that PAD4-mediated NET accumulation promotes kidney injury (Rabadi et al., 2019; Raup-Konsavage et al., 2018) and potentially renal fibrosis (Martinod et al., 2017). However, the specific pathogenic and regulatory roles and mechanisms of NETs in renal fibrosis and the fibrotic microenvironment are not completely understood.

Here, we uncovered that accumulated NETs in the kidneys were associated with worsened renal function in ON patients. NETs promoted macrophage expression of CXCL9/10/11 thus facilitating the infiltration of cytotoxic $CD8^+$ T cells, which produced granzyme B to mediate kidney fibrosis.

Results

NETs were accumulated in ON patients and correlated with kidney function loss

We previously performed a proteomic study of obstruction-induced renal fibrosis in ON patients (Fig. 1A and 1B) (Tao et al., 2023). Of note, proteins that were upregulated in the fibrotic kidneys were significantly enriched in the neutrophil extracellular trap formation pathway (Fig. 1C), which was further validated by the heightened expression of the NET marker CitH3 in the fibrotic kidneys from ON patients (Fig. 1D and 1E). We then detected the circulating levels of NET components in ON patients (Fig. 1F). Interestingly, ON patients displayed elevated circulating levels of NET components compared to healthy controls, including double-stranded DNA (dsDNA), DNA-histone complexes, and neutrophil elastase (NE) (Fig. 1G). Additionally, querying publicly available datasets (GSE66494) (Chen et al., 2023) showed an increase in *PADI4* (encoding PAD4) expression in kidneys from CKD patients (Fig. 1H). Taken together, these data indicate the accumulation of NETs in ON patients.

Next, we assessed the clinical relevance of NETs in patients by analyzing the correlation between circulating NET components and the glomerular filtration rate (GFR) of the obstructed kidneys (Fig. 1F). We collected 41 ON patients who had received MAG3 renograms that provided the GFR of the right and left kidneys (Table S1). The patients were divided into two groups based on the split renal function (SRF), which represents the relative contribution of each of the two kidneys to total renal function. We used 40% as the cut-off because patients with less than 40% SRF are recommended to undergo surgical correction (Jackson et al., 2018). Notably, the circulating dsDNA levels were significantly higher in patients with <40% SRF compared to patients with >40%

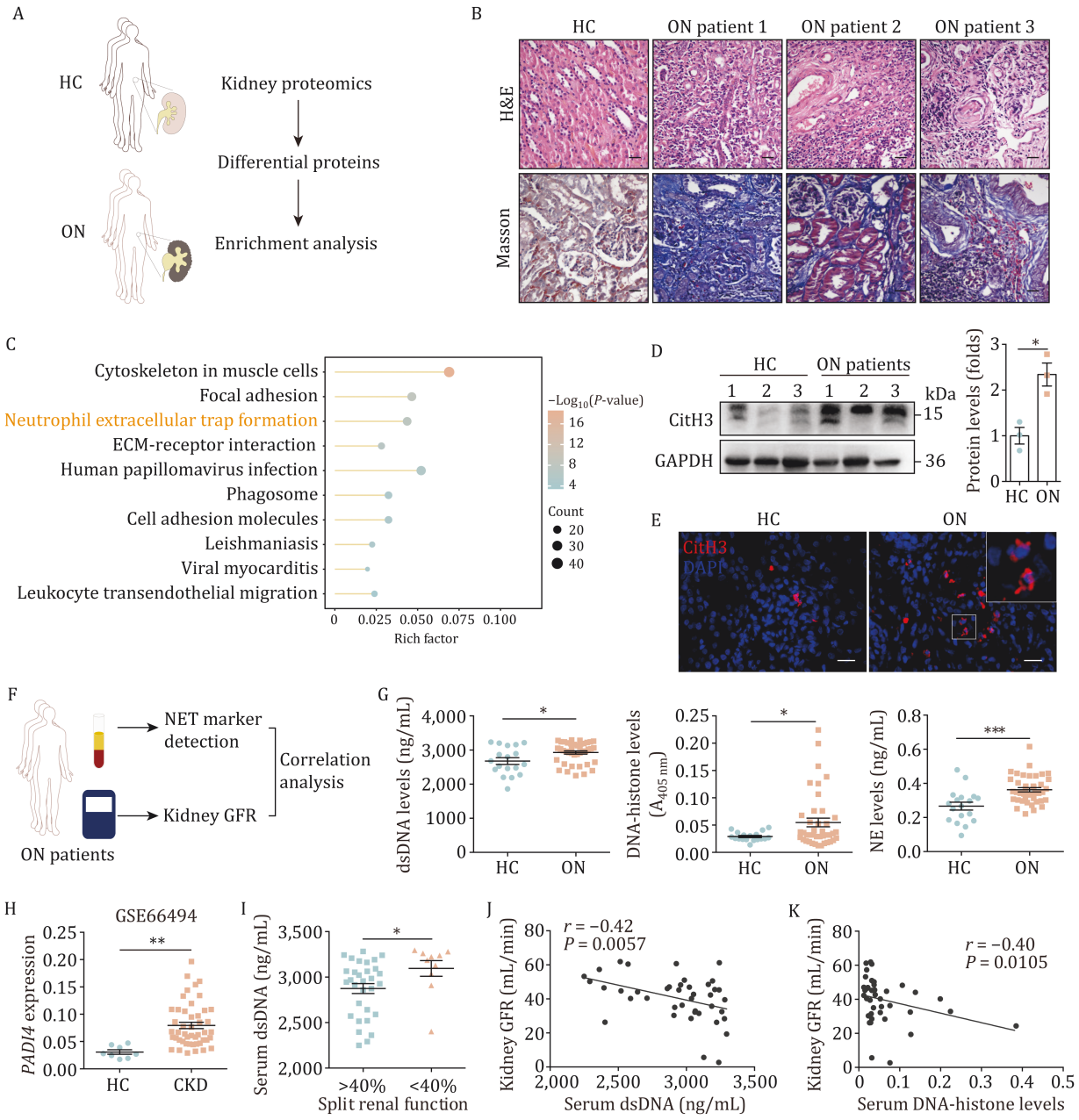

Figure 1. NETs were accumulated in ON patients and correlated with kidney function loss. (A) The schematic of the experimental design. (B) Representative H&E and Masson staining of kidneys from healthy control and ON patients. Scale bars 20 μm. (C) Kyoto Encyclopedia of Genes and Genomes (KEGG) analysis of the proteins that were upregulated in human fibrotic kidneys compared with control kidneys. The top 10 enriched pathways were shown. (D) Immunoblots and quantification for CitH3 in kidneys from healthy control (HC) and ON patients ($n = 3$). (E) Representative immunofluorescence for CitH3 in kidneys from healthy controls and ON patients. Scale bars 20 μm. (F) The schematic of the experimental design. (G) Serum samples from healthy controls and ON patients were analyzed to quantify the circulating levels of dsDNA, DNA-histone complexes, and NE ($n = 18/41$). (H) *PADI4* expression in healthy controls and CKD patients was analyzed by querying publicly available data ($n = 8/48$). (I) Serum dsDNA levels were shown in patients <40% SRF and patients >40% SRF ($n = 31/10$). Spearman correlation between the GFR of the obstructed kidneys and (J) serum levels of dsDNA and (K) DNA-histone complexes ($n = 41$). The results represent mean ± SEM. * $P < 0.05$, ** $P < 0.01$, *** $P < 0.001$.

SRF (Fig. 1I). Moreover, the SRF of the obstructed kidneys was negatively correlated with serum dsDNA levels ($r = -0.42$, $P = 0.0057$) and DNA-histone complexes ($r = -0.40$, $P = 0.0105$) (Fig. 1J and 1K). These results suggest that NETs are associated with worsened renal function in ON patients.

NETs were present in murine obstructed kidneys and promoted UUO-induced renal fibrosis

To translate the human results into murine models, we utilized the UUO mouse model, a well-established animal ON model. We observed an increased infiltration of neutrophils into UUO kidneys (Fig. S1A). Proteomic

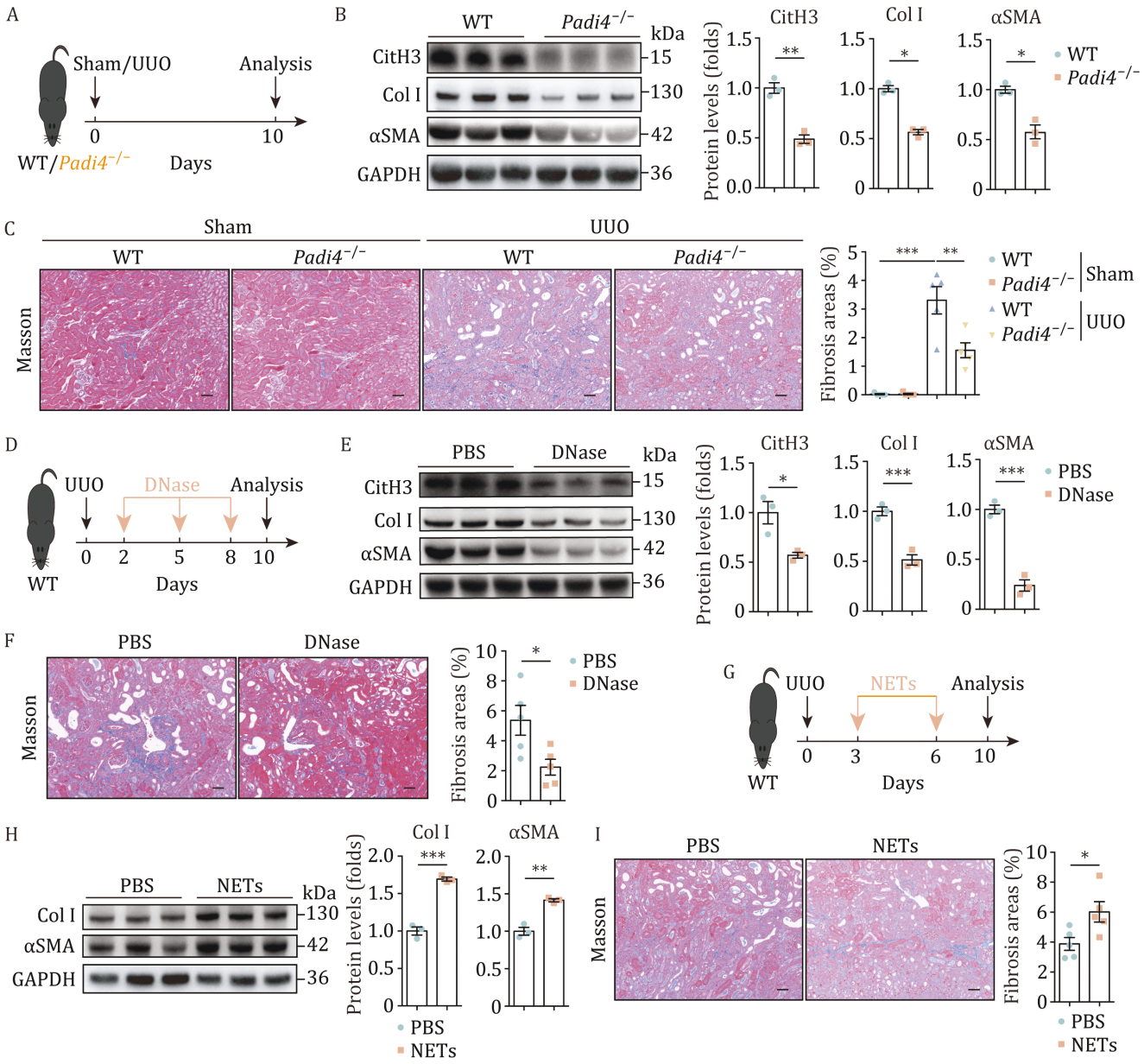

Figure 2. NETs promoted UUO-induced renal fibrosis. (A) The schematic of the experimental design. (B) Immunoblots and quantification for CitH3, Col I, and αSMA in UUO kidneys from WT and *Padi4*$^{-/-}$ mice ($n = 3$). (C) Representative Masson staining and quantification of kidneys in WT and *Padi4*$^{-/-}$ mice subjected to sham or UUO operation ($n = 5$). Scale bars 50 μm. (D) The schematic of the experimental design. (E) Immunoblots and quantification for CitH3, Col I, and αSMA in UUO kidneys from PBS- or DNase-treated mice ($n = 3$). (F) Representative Masson staining and quantification of UUO kidneys in PBS- or DNase-treated mice ($n = 5$). Scale bars 50 μm. (G) The schematic of the experimental design. (H) Immunoblots and quantification for Col I and αSMA in UUO kidneys from PBS- or NET-transferred mice ($n = 3$). (I) Representative Masson staining and quantification of UUO kidneys in PBS- or NET-transferred mice ($n = 5$). Scale bars 50 μm. The results represent mean ± SEM. * $P < 0.05$, ** $P < 0.01$, *** $P < 0.001$.

profiling revealed that proteins that were increased in UUO kidneys were enriched in pathways associated with NET formation, neutrophil migration, activation, degranulation, and cytotoxicity (Fig. S1B–D). Consistent with the findings in ON patients, we confirmed that NETs were accumulated in mouse obstructed kidneys as well (Fig. S1E and S1F).

To investigate the pathogenic role of NETs in ON development, we took advantage of *Padi4*$^{-/-}$ mice in which NET formation was inhibited (Papayannopoulos, 2018) (Fig. 2A). We confirmed the knockout effectiveness by immunoblots (Fig. S2A). Indeed, PAD4-deficient mice displayed impaired NET formation as reflected by the decreased circulating levels of NET components, including dsDNA and myeloperoxidase (MPO)-DNA (Fig. S2B). Of note, PAD4-deficient mice exhibited decreased expression of the fibrosis markers collagen I (Col I) and α smooth muscle actin (αSMA) in UUO kidneys compared to wild-type

(WT) controls (Fig. 2B). Moreover, PAD4 deficiency led to decreased collagen deposition in the obstructed kidneys, while PAD4 deletion resulted in little histological change in sham kidneys (Fig. 2C). PAD4-deficient mice also showed a decline in blood urea nitrogen (BUN) and serum creatinine levels, implying that PAD4 deletion was renoprotective in UUO kidneys (Fig. S2C). DNase is another well-described strategy to block NET formation (Warnatsch et al., 2015). We found that DNase treatment resulted in decreased Col I and αSMA expression, reduced collagen deposition (Fig. 2D–F), and downregulated injury marker *Kim1* in UUO kidneys (Fig. S2D). These data demonstrate that genetic or pharmacological inhibition of NETs protects against obstruction-induced kidney fibrosis and injury.

To further ascertain the pathogenic role of NETs in UUO kidneys, we used the strategy of NET adoptive transfer (Fig. 2G). The isolated bone marrow-derived neutrophils were stimulated with PMA to form NETs *in vitro* (Fig. S2E), which were then transferred into UUO mice intravenously. In contrast to PAD4 deletion or DNase treatment, NET transfer contributed to increased levels of Col I and αSMA, as well as larger collagen-positive areas in UUO kidneys (Fig. 2H and 2I). Moreover, compared to the controls, mice that received NET-transfer expressed higher levels of *Tgfb1*, the master regulator of renal fibrosis (Fig. S2F). Collectively, these data support a pathogenic role for NETs in driving obstruction-induced renal fibrosis.

NETs promoted kidney inflammation and T-cell accumulation in UUO kidneys

To investigate the mechanisms underlying NET regulation on renal fibrosis, we performed bulk RNA sequencing (RNA-seq) analysis of UUO kidneys from WT and *Padi4*$^{-/-}$ mice. RNA-seq revealed 170 upregulated and 250 downregulated genes in PAD4-deficient mice compared to WT mice ($P < 0.05$, fold change > 1.5). Notably, Gene Ontology (GO) analysis showed that the downregulated genes in *Padi4*$^{-/-}$ mice were significantly enriched in inflammation-associated pathways, such as leukocyte cell-cell adhesion, adaptive immune response, positive regulation of T-cell activation, and leukocyte migration (Fig. 3A). Moreover, KEGG enrichment suggested that cell adhesion molecules, T-cell receptor signaling pathway, cytokine-cytokine receptor interaction, IL-17 signaling, and Th17 cell differentiation were inhibited in *Padi4*$^{-/-}$ mice (Fig. 3B). Furthermore, we noticed that PAD4-deficient mice exhibited a significant decrease in inflammatory cytokines, such as *Il1b*, *Il6*, and *Il33* (Fig. 3C). *Itgal*, which is involved in the adhesion and transmigration of T cells and neutrophils (Ostermann et al., 2002), was diminished due to PAD4 deletion (Fig. 3C). We then confirmed that the inflammatory cytokines *Il1b* and *Tnf* were downregulated after NET inhibition, while they were upregulated after NET transfer (Fig. 3D–F). These results suggest that NETs promote inflammation, especially T-cell immunity, in UUO kidneys.

Given that NETs are critical regulators of inflammation (Papayannopoulos, 2018) and T-cell response was among the top 10 downregulated pathways in *Padi4*$^{-/-}$ mice (Fig. 3B), we next sought to assess the impact of NETs on renal immune cells, especially T cells (Fig. S3A). Flow cytometry analysis showed that PAD4-deficient mice displayed significantly reduced infiltration of T cells and neutrophils into UUO kidneys compared with WT controls (Figs. 3G–I and S3B–D). This was consistent with the RNA-seq analysis showing that leukocyte migration and T-cell immunity were blunted after PAD4 deletion (Fig. 3A and 3B). Interestingly, PAD4 deletion did not significantly affect renal infiltration of monocytes, macrophages, dendritic cells, B cells, natural killer (NK) cells, or natural killer T (NKT) cells (Figs. 3I and S3B–D). Similarly, DNase treatment resulted in less infiltration of T cells into UUO kidneys, while other immune cells, especially neutrophils, were rarely affected (Figs. 3J and S3E–H). Moreover, NET transfer contributed to enhanced recruitment of T cells instead of other cells, including neutrophils (Figs. 3K and S3I–K). Therefore, these data demonstrate that NETs promote the accumulation of T cells in the obstructed kidneys.

NETs facilitated cytotoxic CD8$^+$ T cell infiltration into UUO kidneys

Next, we examined the patterns of NET regulation on T cells during renal fibrosis. We mined the RNA-seq data and revealed a decrease in T-cell (especially CD8$^+$ T-cell) associated genes in *Padi4*$^{-/-}$ mice, such as *Cd3e*, *Cd8a*, and *Cd8b1* (Fig. 4A). PAD4 deficiency also led to a reduction in *Lck* and *Cd28* expression, which are required for T-cell activation (Fig. 4A). Importantly, PAD4-deficient mice showed a significantly reduced expression of *Gzmb* (encoding granzyme B, GZMB), the key effector molecule in cytotoxic CD8$^+$ T cells (Fig. 4A). Thus, transcriptome analysis suggests that NETs may be critical regulators of CD8$^+$ T cells during UUO-induced renal fibrosis.

We then performed a flow cytometry analysis in three different settings to analyze CD4$^+$ and CD8$^+$ T cells in the tissue microenvironment. Notably, PAD4 deficiency or DNase treatment resulted in less infiltration of CD4$^+$ and CD8$^+$ T cells into UUO kidneys, whereas NET transfer contributed to an increase in CD8$^+$ T cells, but not CD4$^+$ T cells (Fig. 4B). Moreover, GZMB-expressing CD8$^+$ T cells were remarkably reduced in *Padi4*$^{-/-}$ mice or DNase-treated mice, whereas they were elevated in NET-transferred mice compared to the controls (Fig. 4C). Consistently, immunoblots showed that GZMB expression was inhibited by PAD4 deletion and DNase treatment, while NET transfer resulted in elevated GZMB levels in UUO kidneys (Fig. 4D). Perforin is the major effector molecule of

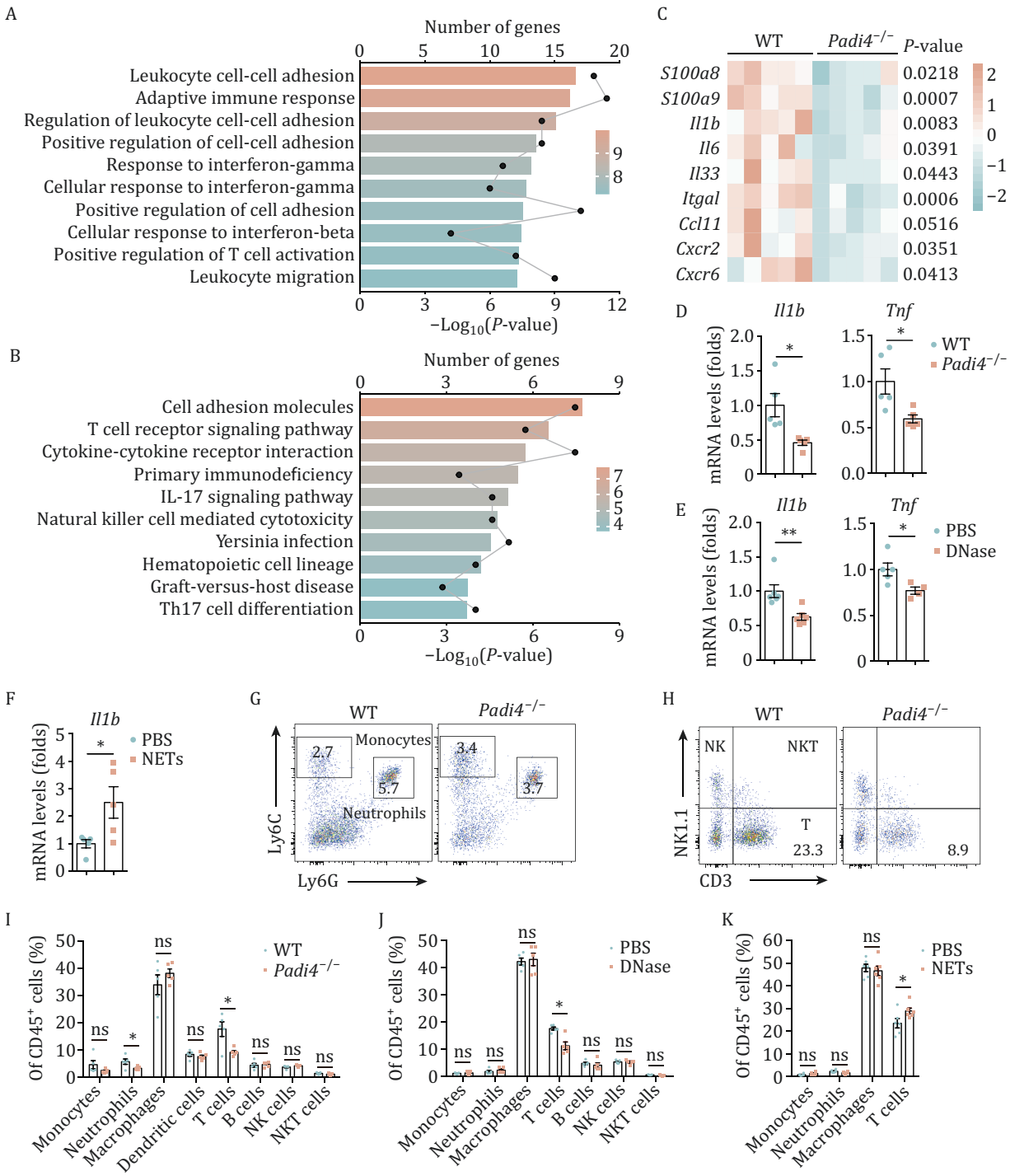

Figure 3. NETs promoted kidney inflammation and T-cell infiltration. (A) The top 10 GO biological processes enriched in the downregulated genes in PAD4-deficient mice versus WT mice. The points indicate the number of genes, and the bars and colors indicate *P*-value. (B) The top 10 KEGG pathways enriched in the downregulated genes in PAD4-deficient mice. The points indicate the number of genes, and the bars and colors indicate *P*-value. (C) Heatmap showing differentially expressed genes involved in kidney inflammation. Each column represents a single sample ($n = 5$). The *P*-value between the two groups was analyzed. qPCR analysis for *Il1b* or *Tnf* in UUO kidneys from (D) WT/PAD4-deficient, (E) PBS/DNase-treated, and (F) PBS/NET-transferred mice ($n = 4$ to 6). Representative flow cytometry plots of (G) monocytes ($CD11b^+$ $F4/80^-$ $Ly6C^+$) and neutrophils ($CD11b^+$ $F4/80^-$ $Ly6G^+$) and (H) NK ($CD3^-$ $NK1.1^+$), NKT ($CD3^+$ $NK1.1^+$), and T cells ($CD3^+$) in UUO kidneys from WT/*Padi4*$^{-/-}$ mice. Quantification of renal immune cells in UUO kidneys from (I) WT/*Padi4*$^{-/-}$ ($n = 5$), (J) PBS/DNase-treated ($n = 5$), and (K) PBS/NET-transferred mice ($n = 6$). The results represent mean ± SEM. * $P < 0.05$, ** $P < 0.01$, ns, no significance.

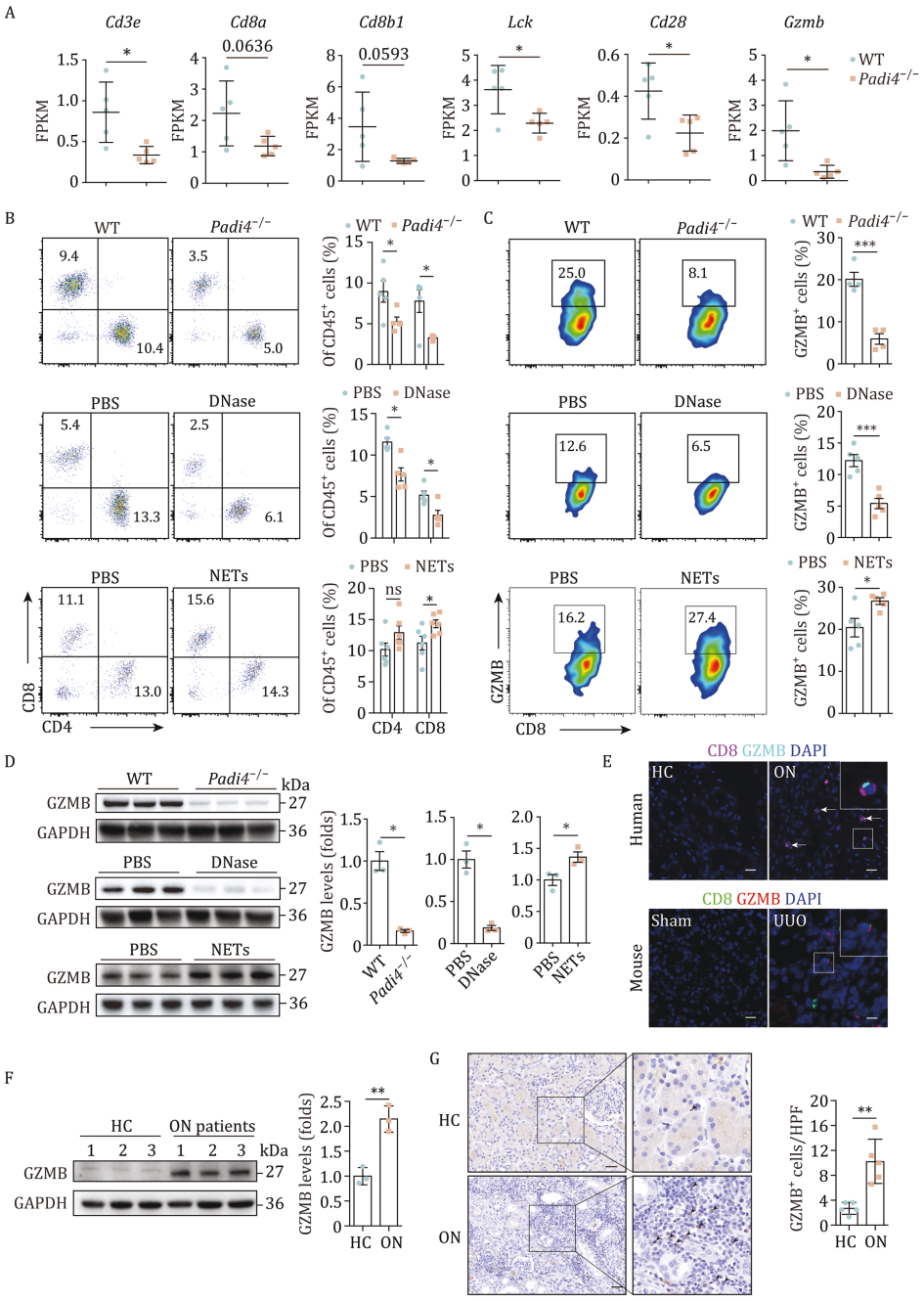

Figure 4. NETs facilitated the accumulation of cytotoxic CD8⁺ T cells. (A) Expression levels of differential T cell-associated genes in UUO kidneys from WT and *Padi4*$^{-/-}$ mice in the RNA-seq analysis ($n = 5$). Gene expression was quantified by FPKM (fragments per kilobase per million mapped reads). (B) Representative flow cytometry plots (Gated on kidney CD3⁺ cells) and quantification of CD4⁺ and CD8⁺ T cells in UUO kidneys from WT/*Padi4*$^{-/-}$ ($n = 5$), PBS/DNase-treated ($n = 5$), and PBS/NET-transferred mice ($n = 6$). (C) Representative flow cytometry plots (Gated on kidney CD3⁺ CD8⁺ cells) and quantification of GZMB-expressing CD8⁺ cells in UUO kidneys from WT/*Padi4*$^{-/-}$ ($n = 4$), PBS/DNase-treated ($n = 5$), and PBS/NET-transferred mice ($n = 5$). (D) Immunoblots and quantification for GZMB in UUO kidneys from WT/*Padi4*$^{-/-}$, PBS/DNase-treated, and PBS/NET-transferred UUO mice ($n = 3$). (E) Representative immunofluorescence of CD8 and GZMB in control and obstructed kidneys from human and mice. Scale bars 20 μm. The arrows indicate GZMB⁺ CD8⁺ cells. (F) Immunoblots and quantification for GZMB in kidneys from healthy control and ON patients ($n = 3$). (G) Representative immunohistochemistry staining and quantification of GZMB in kidneys from healthy control and ON patients. Scale bars 40 μm. The results represent mean ± SEM. * $P < 0.05$, ** $P < 0.01$, *** $P < 0.001$, ns, no significance.

CD8⁺ T cells that helps GZMB enter target cells to induce apoptosis (Voskoboinik et al., 2015). However, we did not observe significant changes in perforin expression in CD8⁺ T cells after PAD4 deletion or DNase treatment (Fig. S4A). We then observed the presence of GZMB⁺ CD8⁺ T cells by immunofluorescence analysis in the obstructed kidneys from both ON patients and UUO mice (Fig. 4E). Importantly, the obstructed kidneys from ON patients

(Fig. 4F and 4G) and UUO mice (Fig. S4B) exhibited a significant increase in GZMB expression compared to the control. Furthermore, we treated activated CD8⁺ T cells with NETs *in vitro*, and the results showed that NETs induced the expression of GZMB but not perforin in CD8⁺ T cells (Fig. S4C). Overall, these data suggest that NETs facilitate the accumulation of GZMB⁺ CD8⁺ T cells during renal fibrosis.

To examine whether NETs regulate CD4⁺ T cell response, we analyzed Th1, Th2, and Th17 cells in UUO kidneys. Interestingly, PAD4 deficiency led to slightly but significantly reduced T-bet in CD4⁺ T cells, the key transcription factor driving Th1 cell differentiation, while GATA3 expression was rarely affected (Fig. S4D). This indicates that NETs may influence Th1 response in UUO-induced renal fibrosis. We observed no significant alterations in *Il17a* expression in UUO kidneys from PAD4-deficient, DNase-treated, or NET-transferred experiments (Fig. S4E), although RNA-seq data exhibited downregulation of IL17/Th17 signaling in *Padi4*$^{-/-}$ mice (Fig. 3B).

CD8⁺ T cell-derived GZMB promoted renal fibrosis by inducing tubular cell EMT and fibroblast activation

GZMB, produced by cytotoxic CD8⁺ T cells, induces cell apoptosis through caspase-dependent pathways (Velotti et al., 2020). Interestingly, recombinant GZMB alone cannot trigger significant cleavage of caspase-3 in TCMK-1 cells (a murine tubular cell line) (Fig. 5A). In contrast, the combination of GZMB and recombinant human TGF-β (rhTGF-β) resulted in elevated levels of cleaved caspase-3 (Fig. 5A). As a comparison, TCMK-1 apoptosis was not affected by NETs (Fig. S5A).

Given that granzyme is reported to be able to induce EMT through non-cytotoxic mechanisms (Tiberti et al., 2022; Velotti et al., 2020) and tubular cell EMT is a key step in kidney fibrosis development (Li et al., 2022a), we hypothesized that extracellular GZMB may promote renal fibrosis by regulating EMT. Of note, recombinant GZMB promoted the EMT process in TCMK-1 cells *in vitro*, as evidenced by the upregulation of fibronectin (FN), Col I, and αSMA and the downregulation of E-Cadherin (E-Cad) (Fig. 5A). Additionally, we observed that NETs cannot elicit the EMT process in TCMK-1 cells (Fig. S5A). We also examined whether GZMB was responsible for fibroblast activation. Importantly, GZMB induced Col I and αSMA expression in NIH-3T3 cells (Fig. 5B), whereas NETs cannot (Fig. 5B). Taken together, these data suggest that CD8⁺ T cell-produced GZMB drives tubular EMT and fibroblast activation, but NETs may not directly mediate these processes in our settings.

To understand the role of GZMB *in vivo*, we used a GZMB inhibitor Z-IETD-FMK (FMK) (Xu et al., 2024) (Fig. 5C). FMK significantly inhibited UUO-induced renal fibrosis as revealed by decreased Col I and αSMA expression and smaller collagen-positive areas in the obstructed kidneys (Fig. 5D and 5E). Moreover, the expression of the epithelial marker, E-Cad, was promoted by GZMB inhibition (Fig. 5D). These data suggest that FMK inhibits the tubular EMT process. FMK also led to reduced levels of *Tgfb1*, *Kim1*, and *Ngal* in UUO kidneys (Fig. 5F). Furthermore, FMK-treated mice displayed a significant reduction in the renal expression of pro-inflammatory cytokines, including *Il1b*, *Tnf*, and *Mcp1* (Fig. 5G). Thus, these findings suggest that pharmacological inhibition of GZMB alleviated renal fibrosis partially by blunting tubular EMT in UUO kidneys.

NETs potentiated macrophage production of CXCL9/10/11 to recruit CD8⁺ T cells

Then, we asked about how NETs regulated CD8⁺ T cell accumulation during renal fibrosis. We first examined whether NETs affect the renal expression of T cell-recruiting chemokines. Importantly, in CKD patients, renal *GZMB* was positively correlated with *CXCL9/10/11* expression (Fig. S6A), the primary chemokines attracting T cells (Hoch et al., 2022), suggesting that these chemokines were critical in the infiltration of cytotoxic CD8⁺ T cells. We further found that the serum levels of CXCL9/10 were significantly elevated in ON patients compared to healthy controls (Fig. 6A). Interestingly, *CXCL11* was upregulated in a publicly available CKD datasets (GSE66494) (Chen et al., 2023) (Fig. S6B). In animal experiments, PAD4 deficiency resulted in reduced protein levels of CXCL9/10 in UUO kidneys (Fig. 6B). Moreover, the levels of *Cxcl9/10/11* in UUO kidneys were remarkably reduced after PAD4 deletion or DNase treatment, whereas NET transfer led to an increase in *Cxcl9/10*, but not *Cxcl11* (Fig. 6C–E). Together, these data suggest that NETs promote the production of T-cell chemokines during renal fibrosis, which is supposed to be responsible for the CD8⁺ T cell accumulation in the obstructed kidneys.

Macrophages are the primary sources of T cell-attracting chemokines (House et al., 2020). Interestingly, F4/80-positive macrophages in UUO kidneys expressed remarkably higher levels of *Cxcl9/10/11* compared to F4/80-negative cells (3.7- to 14.8-fold increase) (Fig. 6F and 6G), suggesting that T-cell recruiting chemokines were mainly produced by macrophages. Of note, immunofluorescence analysis revealed that NETs were present in proximity to macrophages in the obstructed kidneys from both ON patients and UUO mice (Fig. 6H). Therefore, we presumed that NETs may induce T-cell chemokines in macrophages. We found that PAD4 deletion or DNase treatment dramatically diminished *Cxcl9/10/11* expression in macrophages isolated from UUO kidneys (Fig. 6F and 6G), suggesting that NETs drive the production of these chemokines. We then performed experiments to study whether NETs induce *Cxcl9/10/11* expression in bone marrow-derived macrophages (Fig. 6I and 6J). Notably, NETs profoundly induced macrophage

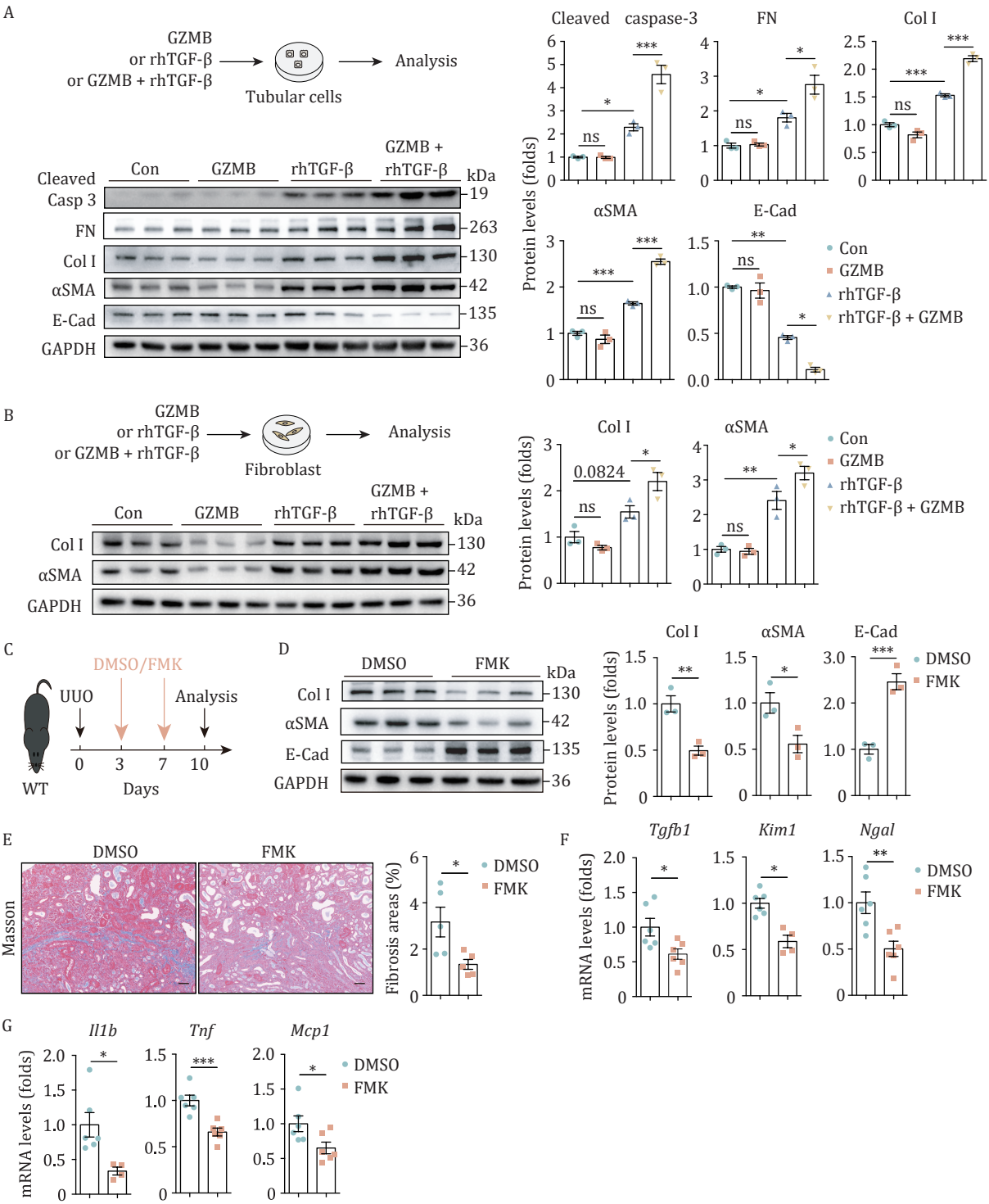

Figure 5. CD8⁺ T cell-derived GZMB promoted renal fibrosis by inducing tubular cell EMT and fibroblast activation. (A) Immunoblots and quantification for cleaved caspase-3, FN, Col I, αSMA, and E-Cad in TCMK-1 cells treated with or without recombinant GZMB and rhTGF-β ($n = 3$). (B) Immunoblots and quantification for Col I and αSMA in NIH-3T3 cells treated with or without recombinant GZMB and rhTGF-β ($n = 3$). (C) The schematic of the experimental design. (D) Immunoblots and quantification for Col I, αSMA, and E-Cad in UUO kidneys from DMSO- or FMK-treated mice ($n = 3$). (E) Representative Masson staining and quantification of UUO kidneys from mice treated with or without FMK ($n = 5$). Scale bars 50 μm. qPCR analysis for (F) *Tgfb1*, *Kim1*, and *Ngal*, and (G) *Il1b*, *Tnf*, and *Mcp1* in UUO kidneys from DMSO- and FMK-treated UUO mice ($n = 4$ to 6). The results represent mean ± SEM. * $P < 0.05$, ** $P < 0.01$, *** $P < 0.001$, ns, no significance.

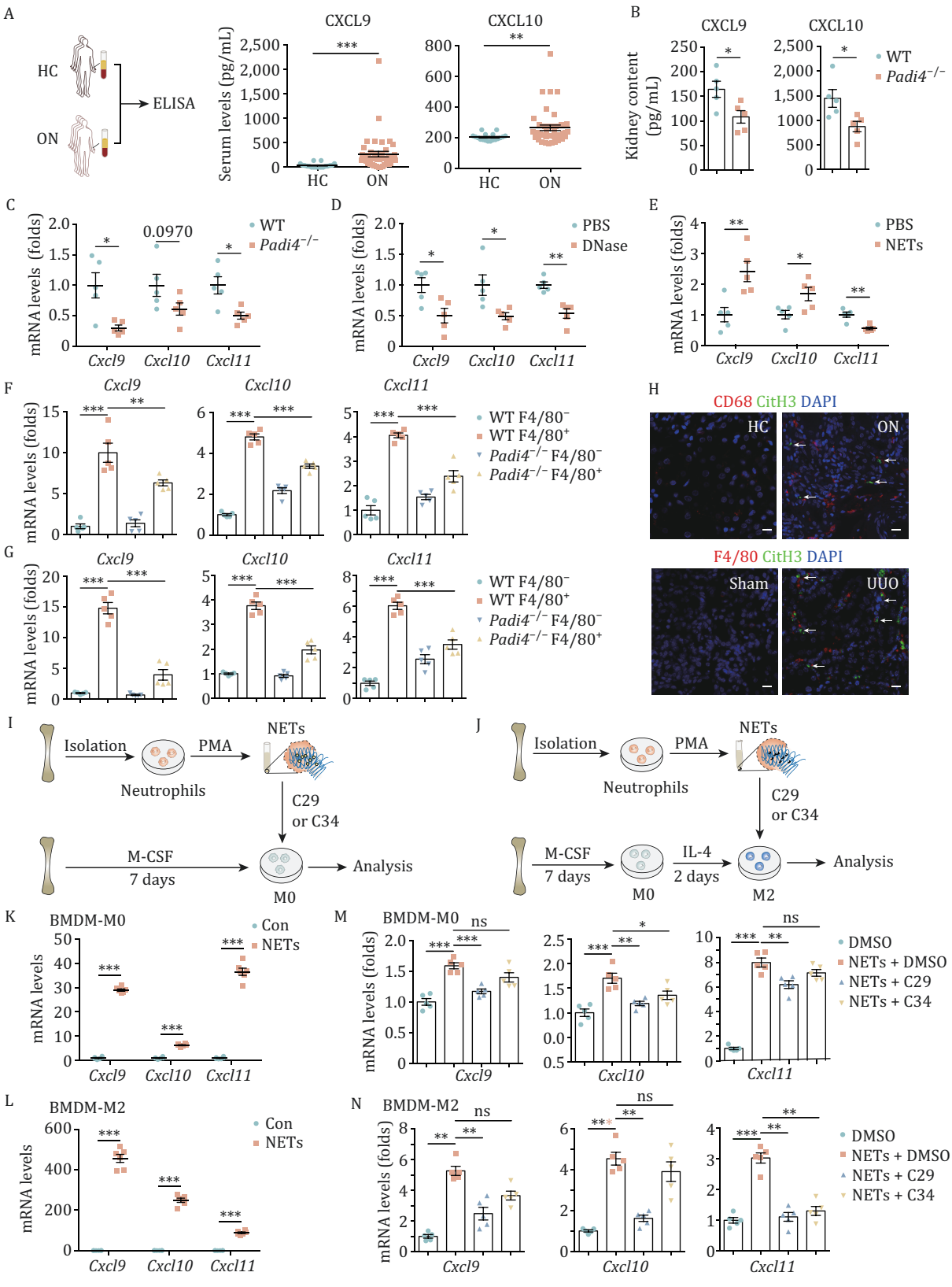

Figure 6. NETs potentiated macrophage production of CXCL9/10/11 to recruit CD8⁺ T cells. (A) Serum levels of CXCL9/10/11 in healthy control and ON patients (n = 18/41). (B) UUO kidneys from WT/*Padi4*$^{-/-}$ mice were homogenized and CXCL9/10 concentrations were detected by ELISA (n = 5). qPCR analysis for *Cxcl9/10/11* expression in UUO kidneys from (C) WT/*Padi4*$^{-/-}$, (D) PBS/DNase-treated, and (E) PBS/NET-transferred mice (n = 5). qPCR analysis for *Cxcl9/10/11* expression in isolated F4/80^{-} and F4/80^{+} cells in the UUO kidneys from (F) WT/*Padi4*$^{-/-}$ or (G) PBS/DNase-treated mice (n = 5). (H) Representative immunofluorescence images of CD68 and

expression of *Cxcl9/10/11*, regardless of whether they were M0 or IL-4-activated M2 macrophages (Fig. 6K and 6L). Mechanistically, the induction of *Cxcl9/10/11* could be partially eliminated by the TLR2 inhibitor in M0 or IL-4-activated M2 macrophages (Fig. 6M and 6N). Additionally, the TLR4 inhibitor blunted *Cxcl10* in M0 and *Cxcl11* in M2 macrophages (Fig. 6M and 6N). This is consistent with previous studies documenting that NETs signal through the TLR2/4 pathway when interacting with other immune cells (Kim et al., 2023; Warnatsch et al., 2015; Wilson et al., 2022). However, NETs cannot induce CXCL9/10/11 expression in TCMK-1 or NIH-3T3 cells (Fig. S6C and S6D). These results demonstrate that NETs potentiate macrophage production of T cell-recruiting chemokines to facilitate $CD8^+$ T cell infiltration, partially through the TLR2/4 signaling.

Next, we assessed whether $CD8^+$ T cell activation could be directly mediated by NETs. We noted that NET treatment resulted in no significant alterations of activation markers in $CD8^+$ T cells, including CD25, CD44, CD69, and GZMB (Fig. S6E), indicating that NETs might not be directly involved in the activation of $CD8^+$ T cells. Moreover, PAD4-deficient mice exhibited fewer Ki67-positive $CD4^+$ and $CD8^+$ T cells in UUO kidneys compared to WT controls, while NET transfer had little effect on T cell proliferation (Fig. S6F), suggesting that T cell proliferation capabilities may be impaired due to PAD4 deletion. Taken together, these data suggest that NETs promote the recruitment of $CD8^+$ T cells instead of activation in the obstructed kidneys.

Discussion

Although considerable evidence demonstrates that inflammation plays a central role in the initiation and progression of obstructive nephropathy and renal fibrosis, little is known about how local immune cells coordinate to drive this condition. Here, we identified that the collaboration between NETs and macrophages regulated $CD8^+$ T cell infiltration and orchestrated obstruction-induced renal fibrosis.

Neutrophil infiltration is a hallmark of CKDs and predicts end-stage renal disease (Heinzelmann et al., 1999; Yuan et al., 2019), but how neutrophils drive the development of CKDs and kidney fibrosis remains largely unknown. It has recently been shown that Siglec F-positive neutrophils are crucial for creating a pro-fibrotic microenvironment in UUO kidneys by producing inflammatory cytokines and collagens (Ryu et al., 2022). Of note, NET is an alternative and important way for neutrophils to exert their functions (Papayannopoulos, 2018). Despite previous studies reporting that NETs mediate kidney injury (Salazar-Gonzalez et al., 2019) and fibroblast activation (Chrysanthopoulou et al., 2014), we observed that NETs cannot trigger apoptosis and EMT in TCMK-1 cells or activation in NIH-3T3 cells. Instead, we utilized multiple approaches to demonstrate a pathogenic role for NETs in orchestrating T-cell inflammation during renal fibrosis.

NETs are critical regulators of inflammation by directly or indirectly interacting with other immune cells, including macrophages and T cells (Warnatsch et al., 2015). Recently, NET-macrophage interaction has been proposed to mediate macrophage-to-myofibroblast transition (MMT) in UUO kidneys (Wang et al., 2022). In this study, the authors showed that UUO induces activation of Gasdermin D in neutrophils thus leading to the formation of NETs, which promote MMT and macrophage inflammation by activating p65 translocation into the nucleus (Wang et al., 2022). However, they did not study the participation of T cells in the UUO model. Unlike this study, we presented here that NETs profoundly potentiated macrophage production of T cell-attracting chemokines, which amplified T-cell inflammation, despite the comparable numbers of macrophages in the tissue microenvironment. Furthermore, the interaction between NETs and T cells has also been repeatedly documented. NETs can directly activate T cells to trigger Th17 response through TLR2 signaling to promote bone loss in periodontitis (Kim et al., 2023; Wilson et al., 2022). However, our results implied that NETs might not predominantly affect $CD4^+$ T cell activation and Th17 differentiation under the scenario of UUO-mediated kidney injury, as renal IL-17A levels were comparable after NET inhibition or transfer. We showed that NETs did not trigger significant activation of $CD8^+$ T cells either, at least in our experimental setting. Instead, we demonstrated that NETs promoted T-cell recruitment by inducing T-cell chemokines in macrophages. Notably, a recent study reported that neutrophils are associated with an increase in granzyme K-expressing $CD8^+$ T cells in colorectal tumors (Tiberti et al., 2022), although how neutrophils regulate the infiltration of $CD8^+$ T cells was not unveiled in this study.

NETs have recently emerged as pivotal mediators of fibrosis in various organs by inducing tissue damage, regulating inflammation, and activating fibroblasts, including the lung (Katsoulis et al., 2024), heart (Yang et

CitH3 in kidneys from healthy control and ON patients, and F4/80 and CitH3 and in kidneys from sham and UUO mice. Scale bars 20 μm. (I and J) The schematic of the experimental design. qPCR analysis for *Cxcl9/10/11* expression in (K) M0 BMDMs and (L) IL-4-activated M2 BMDMs that were treated with or without NETs ($n = 5$). qPCR analysis for *Cxcl9/10/11* in (M) M0 BMDMs and (N) IL-4-activated M2 BMDMs that were treated with or without NETs, TLR2-IN-C29 (C29), and TLR4-IN-C34 (C34) ($n = 5$). The results represent mean ± SEM. * $P < 0.05$, ** $P < 0.01$, *** $P < 0.001$, ns, no significance.

al., 2024), and liver (Babuta et al., 2024; Luo et al., 2024). Consistent with these findings, our study highlights the critical role of NETs in renal fibrosis, where they promote macrophage activation and CD8+ T cell recruitment. Collectively, these observations underscore the crucial role of NETs in fibrotic diseases and reinforce their potential as therapeutic targets across diverse organ systems.

The roles of CD8+ T cells in renal fibrosis seem to be complicated and have not been completely elucidated. Several studies using the UUO model suggest that CD8+ T cells may protect against kidney fibrosis (Dong et al., 2016). For example, CD8 knockout exacerbates UUO-induced renal fibrosis by promoting Th2 cell differentiation (Dong et al., 2016). However, the whole-body knockout of CD8 may not only reduce CD8+ T cells but also have an influence on other cells expressing the CD8 molecule, such as dendritic cells. Therefore, the mechanisms underlying CD8 deletion in kidney fibrosis are complicated. It has been proposed that cytotoxic T cells could induce fibroblast apoptosis, although it is unclear whether this effect reduces renal fibrosis (Velotti et al., 2020). However, the cytotoxic effect of GZMB is not specific to fibroblasts but to all surrounding cells in the microenvironment. There is mounting evidence showing a detrimental role of CD8+ T cells in CKDs. In patients with focal segmental glomerulosclerosis, diabetic kidney disease, and lupus nephritis, tissue-resident-memory CD8+ T cells were significantly increased and promoted podocyte injury and glomerulosclerosis (Li et al., 2022b). Tubulointerstitial CD8+ T cells are independently associated with an unfavorable long-term kidney outcome in lupus nephritis (Zhang et al., 2021). Another study reported that podocyte DNA damage causes the accumulation of NKG2D-positive CD8+ T cells, contributing to sustained kidney injury (Nakamichi et al., 2023). In our study, we provided evidence that CD8+ T cell-derived GZMB promoted renal fibrosis by inducing tubular EMT and fibroblast activation. In particular, CD8+ T cell infiltration was tightly regulated by NET-mediated chemokine release in macrophages. Collectively, these intricate findings may be attributed to the various etiologies of CKDs and the heterogeneity and functional diversity of CD8+ T cells, which require further investigation.

We observed that NET transfer has no significant effect on T cell proliferation, while whole-body PAD4 deletion blunted CD4+ and CD8+ T cell proliferation. These findings suggest that T cell intrinsic PAD4 might be involved in T cell proliferation. It has been reported that *Padi4* is expressed in both murine and human T cells and regulates their activation (Liu et al., 2018). PAD4 also shows ectopic expression in various tumors and plays a critical role in cancer cell proliferation (Fan et al., 2014). Moreover, PAD4 regulates proliferation of hematopoietic cells by controlling c-myc expression (Nakashima et al., 2013). However, whether and how intrinsic PAD4 affects T cell proliferation in the context of obstructive nephropathy require further investigation.

GZMB is a serine protease produced by a variety of immune and non-immune cells (Velotti et al., 2020). Our study revealed that GZMB in the UUO kidneys was predominantly from cytotoxic CD8+ T cells. GZMB is a multifunctional molecule capable of regulating apoptosis, inflammation, ECM remodeling, and EMT via perforin-dependent or -independent pathways (Velotti et al., 2020). Notably, recent studies have proposed a critical role for GZMB in heart, lung, and skin fibrosis (Santos-Zas et al., 2021; Turner et al., 2019). Moreover, local GZMB levels are associated with kidney injury and interstitial fibrosis in systemic lupus erythematosus and renal allograft (Kok et al., 2017; Yadav et al., 2023). Our study showed that recombinant GZMB and rhTGF-β combined treatment promoted tubular cell apoptosis. Furthermore, we provided direct evidence that GZMB induced tubular EMT and fibroblast activation, which are two important origins of myofibroblasts during renal fibrosis (Falke et al., 2015). This is consistent with previous studies showing that GZMB is considered an important EMT promoter, although the underlying mechanisms are unclear (Velotti et al., 2020). Interestingly, we noticed that a recent study using imaging mass cytometry showed that renal cytotoxic CD8+ T cells were found to be increased within 30 μm of activated fibroblasts and correlated with serum Cr levels in CKD patients (Asowata et al., 2024), which seems to support our findings. Additionally, GZMB might participate in renal fibrosis in other ways. For example, GZMB can induce the release of TGF-β by cleaving decorin and ECM substrates (Boivin et al., 2012).

In conclusion, our study suggests that the immune crosstalk between innate and adaptive immune cells conspires to drive obstruction-induced kidney inflammation and fibrosis. Targeting NETs might represent a promising therapy for obstruction-induced renal fibrosis.

Materials and methods

Patient samples

The human serum and kidney samples were obtained from The Seventh Medical Center of Chinese PLA General Hospital, with the approval of the Research Ethics Committee of the hospital. Written informed consent was provided by the legal parents. The study collected 41 pediatric patients diagnosed with hydronephrosis caused by ureteropelvic junction obstruction, and the serum samples were obtained. The control group consisted of 18 serum samples collected from pediatric patients undergoing surgical treatment for inguinal hernia. Inguinal hernia was selected as the control condition because it does not involve systemic inflammation or renal dysfunction, ensuring that serum and urinary parameters reflect normal physiology. Furthermore,

inguinal hernia and UPJO share similar age and gender distributions, allowing for a well-matched comparison. These samples were processed using the same protocol as for the UPJO patient group. The clinical information is shown in Table S1. The obstructed kidneys were from patients with late-presented hydronephrosis, and the control kidneys were sampled from the tumor-free kidney cortex in patients with nephroblastoma, as described in our previous study (Tao et al., 2023).

Animal studies

C57BL/6 wild-type mice were from Charles River in Beijing, China (Vital River). *Padi4*$^{-/-}$ mice (Cat. No. NM-KO-190334) on the C57BL/6 background were purchased from Shanghai Model Organisms Center, Inc. (China). All mice were maintained in a specific pathogen-free condition. All animal experimental procedures were approved by the Institutional Animal Care and Utilization Committees of Chinese PLA General Hospital. For the UUO model, male mice between seven- to eight-week-old were used. Generally, a median abdominal incision was conducted after anesthetization and the left ureter was double-ligated. Mice were sacrificed at indicated time points.

For NET inhibition, DNase (10104159001, Sigma) was injected intraperitoneally on day 2, 5, and 8 after UUO surgery at a dose of 2.5 mg/kg as previously described (Wang et al., 2021). For granzyme B inhibition, Z-IETD-FMK (HY-101297, MedChemExpress) was injected peritoneally (4 mg/kg) on day 3 and day 7 after UUO surgery.

Cell lines and cell culture

The murine proximal tubular cell line TCMK-1 and fibroblast cell line NIH-3T3 were from Cell Resource Center, Institute of Basic Medical Sciences (Beijing, China). The cells were cultured in DMEM supplemented with 10% fetal bovine serum. To induce tubular cell EMT or fibroblast activation, the cells were starved for 24 h and then treated with 10 ng/mL of recombinant human TGF-β (HY-P7118, MedChemExpress) for 3 days. In the GZMB experiments, TCMK-1 and NIH-3T3 were treated with 20 ng/mL of mouse granzyme B recombinant protein (140-03, Peprotech). In the NET experiments, TCMK-1 and NIH-3T3 were treated with 200 ng/mL of NETs.

Western blot

Kidney protein extracts were prepared according to standard protocols. Cell lysates were separated by 10% SDS-PAGE and transferred to polyvinylidene difluoride membranes (Millipore). The following primary antibodies were used: rabbit anti-mouse/human CitH3 (ab219407, Abcam), mouse anti-mouse/human α smooth muscle actin (67735-1-Ig, Proteintech), rabbit anti-mouse/human collagen I (72026, CST), rabbit anti-mouse/human E-Cadherin (3195T, CST), mouse anti-mouse/human fibronectin (66042-1-Ig, Proteintech), rabbit anti-mouse/human cleaved caspase-3 (9661S, CST), rabbit anti-mouse/human granzyme B (ab255598, Abcam), anti-mouse PAD4 (ab214810, Abcam), and mouse anti-mouse/human GAPDH (60004-1-Ig, Proteintech).

Renal function detection

Serum blood urea nitrogen (BUN) and creatinine (Cr) levels were detected using a Urea Assay Kit (C013-2-1, Nanjing Jiancheng, China) and a Creatinine Assay kit (C011-2-1, Nanjing Jiancheng, China) according to the manufacturer's instructions.

Immuno-histochemistry and Masson staining

Human and mouse kidneys were fixed in 4% paraformaldehyde and embedded in paraffin. The kidney sections were stained with Masson's trichrome, and rabbit anti-mouse/human granzyme B (ab255598, Abcam). Images of the kidney slides were obtained on a Nano Zoomer Slide Scanner (Hamamatsu Photonics). The percentage of collagen-positive areas was quantified using ImageJ software.

Immunofluorescence

Human and mouse kidneys were fixed in 4% paraformaldehyde and embedded in OCT (Sakura). Eight micrometer frozen sections were prepared using a Cryotome FSE cryostat (Thermo-Fisher Scientific). The sections were blocked with 5% donkey serum. Then, the following primary antibodies were incubated overnight at 4°C: rat anti-mouse F4/80 (ab6640, Abcam), rabbit anti-human/mouse CitH3 (ab219407, Abcam), rabbit anti-human/mouse Granzyme B (ab255598, Abcam), rat anti-mouse Ly6G (127602, Biolegend), rat anti-mouse CD8 (MA1-145, Invitrogen), and mouse anti-human CD68 (ab955, Abcam). Imaging was performed using a Pannoramic MIDI (3DHISTECH).

Kidney leukocyte isolation and flow cytometry analysis

The kidney immune cells were isolated as previously described (Tao et al., 2023). Generally, mouse kidneys under indicated conditions were harvested and cut into pieces followed by a digestion (HBSS supplemented with 0.05% collagenase IV and 2 mmol/L $CaCl_2$) under 37°C for 25 min. Then, the digested tissues were filtered through a 70 μm nylon mesh and were centrifuged at 500 ×*g* for 5 min. The resulting cell suspension was treated with a Fcγ receptor blocker (101320, BioLegend) for 10 min followed by incubating with the following fluorescent antibodies (all from BioLegend but Perforin-FITC): CD45-BV421 (103134), CD11b-FITC (101206), Ly6G-APC/Cyanine7 (127624), Ly6C-PE (128008), F4/80-APC (123116), CD11c-PE/Cyanine7 (117317), MHC II-PE (107607), CD3-PE (100206), CD4-PE/Cyanine7 (116016), CD8a-APC/

Cyanine7 (100713), NK1.1-FITC (156508), CD20-APC (152107), CD44-PerCP/Cyanine5.5 (103031), CD69-FITC (104505), CD25-APC (101909), Ki67-AF488 (151204), Granzyme B-APC (372204), Perforin A-FITC (154309, eBioscience), T-bet-APC (644813), GATA3-AF488 (653807), and 7AAD (420404). To detect transcription factors, a True-Nuclear Transcription Factor Buffer Set (424401, BioLegend) was used. For the detection of intracellular proteins, such as granzyme B, cells were fixed and permeabilized after surface staining. Flow cytometry was performed on a FACSCanto II (BD Biosciences) and data were analyzed using FlowJo software 10.4.

Renal macrophage isolation

Kidney tissues were digested and leukocytes were prepared as aforementioned. Renal macrophages were isolated by using a Mouse F4/80 Positive Selection Kit (100-0659, Stemcell) according to the manufacturer's instruction.

Bone marrow-derived macrophage (BMDM) stimulation

Bone marrow cells were prepared and cultured in DMEM supplemented with 10% fetal bovine serum and M-CSF (20 ng/mL, Peprotech) for macrophage differentiation for 7 days. In some experiments, BMDMs were treated with 24 h of 200 ng/mL NETs, 10 μmol/L TLR2 inhibitor TLR2-IN-C29 (S6597, Selleck), and 10 μmol/L TLR4 inhibitor TLR4-IN-C34 (S0822, Selleck).

$CD8^+$ T cell isolation and stimulation

Spleen $CD8^+$ T cells were isolated using a Mouse Naïve $CD8^+$ T Cell Isolation Kit (19858, Stemcell) according to the manufacturer's instructions. $CD8^+$ T cells (1×10^6 cells/mL) were activated by Mouse T-Activator CD3/CD28 (11452D, Gibco) with 5 ng/mL IL-2 (212-12, Peprotech) and 200 ng/mL NETs for 72 h in 1640 supplemented with 10% fetal bovine serum. Then the expression of CD25, CD44, CD69, and GZMB was analyzed by flow cytometry to detect the activation status of $CD8^+$ T cells. For GZMB detection, PMA, ionomycin, and brefeldin A (Selleck) were added for 4 h before analysis.

Real-time quantitative PCR (qPCR)

Total RNA in kidney tissues and macrophages was extracted using TRIzol (Thermo-Fisher) according to the manufacturer's protocol. Complementary DNA was generated using a PrimeScript RT Reagent Kit (RR037A, Takara). Real-time quantitative PCR was performed using SYBR Green Realtime PCR Master Mix (QPK-201, Toyobo) on a CFX96 Touch Real-Time PCR Detection System (BioRad). The expression of target genes was normalized to the expression of the housekeeping gene, *Gapdh*. Relative gene expression was calculated using the standard $2^{-\Delta\Delta Ct}$ method. The primers are shown in Table S2.

Enzyme-linked immunosorbent assay (ELISA)

Human serum dsDNA levels were detected using a dsDNA Assay Kit (P7581, Invitrogen). Human serum neutrophil elastase (NE) levels were detected by an NE ELISA Kit (SEA181Hu, Cloud-Clone, China). Human serum levels of DNA-histone complexes were detected using a Cell Death Detection ELISA Kit (11774425001, Roche). Mouse serum levels of dsDNA and MPO-DNA were analyzed using a mouse dsDNA ELISA Kit (HB379-Mu, Hnybio, China) and a mouse MPO-DNA ELISA Kit (HB1200-Mu, Hnybio, China), respectively. For the detection of renal CXCL9/10 concentrations, a Mouse CXCL9 ELISA Kit (EK2143/2, Multi Sciences, China) and a Mouse CXCL10 ELISA Kit (EK268/2, Multi Sciences, China) were used, respectively. For the detection of CXCL9/10 concentrations in human serum samples, a Human CXCL9 ELISA Kit (EK1143, Multi Sciences, China) and a Human CXCL10 ELISA Kit (EK168, Multi Sciences, China) were used, respectively. Generally, mouse kidneys were homogenized in 1 mL of cold PBS and then centrifuged. The supernatants were used to detect chemokines according to the manufacturer's instructions.

NET formation and adoptive transfer

Neutrophils were isolated from the mouse bone marrow using a Mouse Neutrophil Enrichment Kit (19762, Stemcell) under the manufacturer's instructions. NETs were generated and isolated as previously described (Wang et al., 2021; Yazdani et al., 2019). The isolated neutrophils (1×10^6 cells/mL) were stimulated with 100 nmol/L phorbol 12-myristate 13-acetate (PMA) (S7791, Selleck) for 4 h. 0.5 μmol/L Sytox Green (425303, BioLegend) was used to confirm NET formation. The fluorescence of Sytox Green was quantified at excitation and emission wavelength at 504/523 nm on a BioTek Synergy MX Multimode Reader. To isolate NETs, samples were centrifuged at 500 ×g for 10 min to remove neutrophils and then 18,000 ×*g* for 15 min to remove debris. After the second centrifugation, the resulting pellet containing NETs was dissolved in PBS. DNA concentration was quantified using a NanoDrop Microvolume Spectrophotometer (Thermo-Fisher). NETs produced from 2×10^6 neutrophils were transferred to one recipient mouse 3 and 6 days after UUO surgery through the tail vein.

RNA sequencing and data analysis

The kidney tissues were from wild-type and *Padi4*$^{-/-}$ mice ($n = 5$) subjected to UUO for 10 days. Total RNA was extracted from kidney tissues using TRIzol (Thermo-Fisher). RNA was qualified and quantified using a NanoDrop and Agilent 2100 Bioanalyzer. Then RNA was amplified and reverse-transcribed to cDNA for library construction. Samples were sequenced on a NovaseqX Plus platform (Novogene, China). Sequencing data were aligned to the mouse reference genome (version mm10).

Differentially expressed genes were analyzed using DESeq2 with five independent replicates using default parameters (Love et al., 2014).

Statistical analyses

Statistical analyses were performed with GraphPad Prism version 6.0c. All experiments were replicated at least three times. The number of biological replicates is indicated in the figure legends. For comparisons between two groups, the two-tailed Student's *t*-test was used for normally distributed data, and the Mann–Whitney non-parametric test was used for non-normally distributed data. One-way ANOVA was used to analyze three or more comparisons. Spearman correlation was used to evaluate relationships between two variables. A *P*-value less than 0.05 was considered significant.

Supplementary data

Supplementary data is available at *Protein & Cell* online https://doi.org/10.1093/procel/pwaf020.

Acknowledgments

The authors thank Dr. Siqi Hu (National Engineering Laboratory for Birth Defects Prevention and Control of Key Technology, Beijing, China), Prof. Weimin Ci and Dr. Xiubin Li (The Third Medical Center of Chinese PLA General Hospital, Beijing, China) for their technical support.

Author contributions

Y.T., H.Z., and X.Z. designed and supervised the study and wrote the paper. H.J., G.Y., and P.L. performed the experiments and analyzed data. R.P., R.J., and Y.W. analyzed circulating NET components in human serum. Y.C., X.Y., and X.D. performed bioinformation analysis. H.C. and L.M. assisted the animal experiments. K.Y., X.Z., Y.Z., X.Z., T.T., X.C., and X.S. collected human samples and information. All authors read and approved the final manuscript.

Funding

This work was supported by the Capital's Funds for Health Improvement (2022-2-5083), the Youth Support Fund of Chinese PLA General Hospital (22QNFC112), the Innovation Talent Fund of Senior Department of Pediatrics, The Seventh Medical Center of Chinese PLA General Hospital (QZX-04-EKCLJH-1), and Guangxi Natural Science Funding (2025GXNSFBA069059).

Conflict of interest

The authors declare that they have no competing interests.

Ethics approval

Human samples and information handling were approved by the Research Ethics Committee of The Seventh Medical Center of Chinese PLA General Hospital. Animal procedures were approved by the Institutional Animal Care and Utilization Committees of The Seventh Medical Center of Chinese PLA General Hospital.

Consent to participate

The authors declare their agreement to participate.

Consent for publication

The authors declare their agreement to publish.

Data availability

RNA-seq datasets have been deposited in the GEO database under accession code GSE272378. The proteomic data were deposited in the ProteomeXchange Consortium (PXD039314) as described in our previous study (Tao et al., 2023).

References

Asowata EO, Romoli S, Sargeant R *et al*. Multi-omics and imaging mass cytometry characterization of human kidneys to identify pathways and phenotypes associated with impaired kidney function. *Kidney Int* 2024;**106**:85–97.

Avery EG, Bartolomaeus H, Rauch A *et al*. Quantifying the impact of gut microbiota on inflammation and hypertensive organ damage. *Cardiovasc Res* 2023;**119**:1441–1452.

Babuta M, Morel C, De Carvalho Ribeiro M *et al*. Neutrophil extracellular traps activate hepatic stellate cells and monocytes via NLRP3 sensing in alcohol-induced acceleration of MASH fibrosis. *Gut* 2024;**73**:1854–1869.

Boivin WA, Shackleford M, Vanden Hoek A *et al*. Granzyme B cleaves decorin, biglycan and soluble betaglycan, releasing active transforming growth factor-β1. *PLoS One* 2012;**7**:e33163.

Chen QQ, Liu K, Shi N *et al*. Neuraminidase 1 promotes renal fibrosis development in male mice. *Nat Commun* 2023;**14**:1713.

Chrysanthopoulou A, Mitroulis I, Apostolidou E *et al*. Neutrophil extracellular traps promote differentiation and function of fibroblasts. *J Pathol* 2014;**233**:294–307.

Dong Y, Yang M, Zhang J *et al*. Depletion of $CD8^+$ T cells exacerbates $CD4^+$ T cell-induced monocyte-to-fibroblast transition in renal fibrosis. *J Immunol* 2016;**196**:1874–1881.

Falke LL, Gholizadeh S, Goldschmeding R *et al*. Diverse origins of the myofibroblast-implications for kidney fibrosis. *Nat Rev Nephrol* 2015;**11**:233–244.

Fan T, Zhang C, Zong M *et al*. Peptidylarginine deiminase IV promotes the development of chemoresistance through inducing autophagy in hepatocellular carcinoma. *Cell Biosci* 2014;**4**:49.

Garcia-romo GS, Caielli S, Vega B *et al*. Netting neutrophils are major inducers of type I IFN production in pediatric systemic lupus erythematosus. *Sci Transl Med* 2011;**3**:73ra20.

Hakkim A, Furnrohr BG, Amann K *et al*. Impairment of neutrophil extracellular trap degradation is associated with lupus nephritis. *Proc Natl Acad Sci U S A* 2010;**107**:9813–9818.

Heinzelmann M, Mercer-Jones MA, Passmore JC. Neutrophils and renal failure. *Am J Kidney Dis* 1999;**34**:384–399.

Hidalgo A, Libby P, Soehnlein O *et al*. Neutrophil extracellular traps: from physiology to pathology. *Cardiovasc Res* 2022;**118**:2737–2753.

Hoch T, Schulz D, Eling N *et al*. Multiplexed imaging mass cytometry of the chemokine milieus in melanoma characterizes features of the response to immunotherapy. *Sci Immunol* 2022;**7**:eabk1692.

House IG, Savas P, Lai J *et al*. Macrophage-derived CXCL9 and CXCL10 are required for antitumor immune responses following immune checkpoint blockade. *Clin Cancer Res* 2020;**26**:487–504.

Jackson L, Woodward M, Coward RJ. The molecular biology of pelvi-ureteric junction obstruction. *Pediatr Nephrol* 2018;**33**:553–571.

Jansen MP, Emal D, Teske GJ *et al*. Release of extracellular DNA influences renal ischemia reperfusion injury by platelet activation and formation of neutrophil extracellular traps. *Kidney Int* 2017;**91**:352–364.

Kalantar-Zadeh K, Jafar TH, Nitsch D *et al*. Chronic kidney disease. *Lancet* 2021;**398**:786–802.

Katsoulis O, Toussaint M, Jackson MM *et al*. Neutrophil extracellular traps promote immunopathogenesis of virus-induced COPD exacerbations. *Nat Commun* 2024;**15**:5766.

Kim TS, Silva LM, Theofilou VI *et al*. Neutrophil extracellular traps and extracellular histones potentiate IL-17 inflammation in periodontitis. *J Exp Med* 2023;**220**:e20221751.

Kok HM, van den Hoogen LL, van Roon JAG *et al*. Systemic and local granzyme B levels are associated with disease activity, kidney damage and interferon signature in systemic lupus erythematosus. *Rheumatol (Oxford)* 2017;**56**:2129–2134.

Li L, Fu H, Liu Y. The fibrogenic niche in kidney fibrosis: components and mechanisms. *Nat Rev Nephrol* 2022a;**18**:545–557.

Li L, Tang W, Zhang Y *et al*. Targeting tissue-resident memory $CD8^+$ T cells in the kidney is a potential therapeutic strategy to ameliorate podocyte injury and glomerulosclerosis. *Mol Ther* 2022b;**30**:2746–2759.

Liu Y. Cellular and molecular mechanisms of renal fibrosis. *Nat Rev Nephrol* 2011;**7**:684–696.

Liu Y, Lightfoot YL, Seto N *et al*. Peptidylarginine deiminases 2 and 4 modulate innate and adaptive immune responses in TLR-7-dependent lupus. *JCI Insight* 2018;**3**:e124729.

Love MI, Huber W, Anders S. Moderated estimation of fold change and dispersion for RNA-seq data with DESeq2. *Genome Biol* 2014;**15**:550.

Luo Y, Fraser L, Jezykowski J *et al*. Interleukin 8-CXCR2-mediated neutrophil extracellular trap formation in biliary atresia associated with neutrophil extracellular trap-induced stellate cell activation. *Hepatology* 2024;**12**:515–530.

Lv W, Booz GW, Wang Y *et al*. Inflammation and renal fibrosis: recent developments on key signaling molecules as potential therapeutic targets. *Eur J Pharmacol* 2018;**820**:65–76.

Martinod K, Witsch T, Erpenbeck L *et al*. Peptidylarginine deiminase 4 promotes age-related organ fibrosis. *J Exp Med* 2017;**214**:439–458.

Nakamichi R, Hishikawa A, Chikuma S *et al*. DNA-damaged podocyte-CD8 T cell crosstalk exacerbates kidney injury by altering DNA methylation. *Cell Rep* 2023;**42**:112427.

NAKASHIMA K, ARAI S, SUZUKI A *et al*. PAD4 regulates proliferation of multipotent haematopoietic cells by controlling c-myc expression. *Nat Commun* 2013;**4**:1836.

Nakazawa D, Kumar SV, Marschner J *et al*. Histones and neutrophil extracellular traps enhance tubular necrosis and remote organ injury in ischemic AKI. *J Am Soc Nephrol* 2017;**28**:1753–1768.

Nakazawa D, Marschner JA, Platen L *et al*. Extracellular traps in kidney disease. *Kidney Int* 2018;**94**:1087–1098.

Ostermann G, Weber KS, Zernecke A *et al*. JAM-1 is a ligand of the β_2 integrin LFA-1 involved in transendothelial migration of leukocytes. *Nat Immunol* 2002;**3**:151–158.

Papayannopoulos V. Neutrophil extracellular traps in immunity and disease. *Nat Rev Immunol* 2018;**18**:134–147.

Rabadi MM, Han SJ, Kim M *et al*. Peptidyl arginine deiminase-4 exacerbates ischemic AKI by finding NEMO. *Am J Physiol Renal Physiol* 2019;**316**:F1180–F1190.

Raup-Konsavage WM, Wang Y, Wang WW *et al*. Neutrophil peptidyl arginine deiminase-4 has a pivotal role in ischemia/reperfusion-induced acute kidney injury. *Kidney Int* 2018;**93**:365–374.

Ruiz-Ortega M, Rayego-Mateos S, Lamas S *et al*. Targeting the progression of chronic kidney disease. *Nat Rev Nephrol* 2020;**16**:269–288.

Ryu S, Shin JW, Kwon S *et al*. Siglec-F-expressing neutrophils are essential for creating a pro-fibrotic microenvironment in the renal fibrosis. *J Clin Invest* 2022;**132**:e156876.

Salazar-Gonzalez H, Zepeda-Hernandez A, Melo Z *et al*. Neutrophil extracellular traps in the establishment and progression of renal diseases. *Medicina (Kaunas)* 2019;**55**:431.

Santos-Zas I, Lemarié J, Zlatanova I *et al*. Cytotoxic $CD8^+$ T cells promote granzyme B-dependent adverse post-ischemic cardiac remodeling. *Nat Commun* 2021;**12**:1483.

Stevens S. Obstructive kidney disease. *Nurs Clin North Am* 2018;**53**:569–578.

Tang S, Zhang Y, Yin SW *et al*. Neutrophil extracellular trap formation is associated with autophagy-related signalling in ANCA-associated vasculitis. *Clin Exp Immunol* 2015;**180**:408–418.

Tao Y, Wang J, Lyu X *et al*. Comprehensive proteomics analysis identifies CD38-mediated NAD^+ decline orchestrating renal fibrosis in pediatric patients with obstructive nephropathy. *Mol Cell Proteomics* 2023;**22**:100510.

Tiberti S, Catozzi C, Croci O *et al*. GZMK^{high} CD8^{+} T effector memory cells are associated with CD15^{high} neutrophil abundance in non-metastatic colorectal tumors and predict poor clinical outcome. *Nat Commun* 2022;**13**:6752.

Turner CT, Lim D, Granville DJ. Granzyme B in skin inflammation and disease. *Matrix Biol* 2019;**75–76**:126–140.

Velotti F, Barchetta I, Cimini FA *et al*. Granzyme B in inflammatory diseases: apoptosis, inflammation, extracellular matrix remodeling, epithelial-to-mesenchymal transition and fibrosis. *Front Immunol* 2020;**11**:587581.

Voskoboinik I, Whisstock JC, Trapani JA. Perforin and granzymes: function, dysfunction and human pathology. *Nat Rev Immunol* 2015;**15**:388–400.

Wang H, Zhang H, Wang Y *et al*. Regulatory T-cell and neutrophil extracellular trap interaction contributes to carcinogenesis in non-alcoholic steatohepatitis. *J Hepatol* 2021;**75**:1271–1283.

Wang Y, Li Y, Chen Z *et al*. GSDMD-dependent neutrophil extracellular traps promote macrophage-to-myofibroblast transition and renal fibrosis in obstructive nephropathy. *Cell Death Dis* 2022;**13**:693.

Wang L, Xu X, Zhang M *et al*. Prevalence of chronic kidney disease in China: results from the Sixth China Chronic Disease and Risk Factor Surveillance. *JAMA Intern Med* 2023;**183**:298–310.

Warnatsch A, Ioannou M, Wang Q *et al*. Neutrophil extracellular traps license macrophages for cytokine production in atherosclerosis. *Science* 2015;**349**:316–320.

Wilson AS, Randall KL, Pettitt JA *et al*. Neutrophil extracellular traps and their histones promote Th17 cell differentiation directly via TLR2. *Nat Commun* 2022;**13**:528.

Wong SL, Demers M, Martinod K *et al*. Diabetes primes neutrophils to undergo NETosis, which impairs wound healing. *Nat Med* 2015;**21**:815–819.

Xu H, Wei Z, Chen B *et al*. Granzyme B PET imaging inflammation and remodeling in myocardial infarction. *Eur J Nucl Med Mol Imaging* 2024;**51**:991–1001.

Yadav B, Prasad N, Agrawal V *et al*. Lower circulating cytotoxic T-cell frequency and higher intragraft granzyme-B expression are associated with inflammatory interstitial fibrosis and tubular atrophy in renal allograft recipients. *Medicina (Kaunas)* 2023;**59**:1175.

Yang K, Gao R, Chen H *et al*. Myocardial reperfusion injury exacerbation due to ALDH2 deficiency is mediated by neutrophil extracellular traps and prevented by leukotriene C4 inhibition. *Eur Heart J* 2024;**45**:1662–1680.

Yazdani HO, Roy E, Comerci AJ *et al*. Neutrophil extracellular traps drive mitochondrial homeostasis in tumors to augment growth. *Cancer Res* 2019;**79**:5626–5639.

Yuan Q, Wang J, Peng Z *et al*. Neutrophil-to-lymphocyte ratio and incident end-stage renal disease in Chinese patients with chronic kidney disease: results from the Chinese Cohort Study of Chronic Kidney Disease (C-STRIDE). *J Transl Med* 2019;**17**:86.

Zhang T, Wang M, Zhang J *et al*. Association between tubulointerstitial CD8^{+}T cells and renal prognosis in lupus nephritis. *Int Immunopharmacol* 2021;**99**:107877.

Zheng F, Ma L, Li X *et al*. Neutrophil extracellular traps induce glomerular endothelial cell dysfunction and pyroptosis in diabetic kidney disease. *Diabetes* 2022;**71**:2739–2750.